

A VLBA Survey of radio stars in the Orion Nebula Cluster: I. The nonthermal radio population

JAN FORBRICH,^{1,2} SERGIO A. DZIB,³ MARK J. REID,² AND KARL M. MENTEN³

¹*Centre for Astrophysics Research, University of Hertfordshire, College Lane, Hatfield AL10 9AB, UK*

²*Center for Astrophysics | Harvard & Smithsonian, 60 Garden St, Cambridge, MA 02138, USA*

³*Max-Planck-Institut für Radioastronomie, Auf dem Hügel 69, D-53121 Bonn, Germany*

Submitted to ApJ

ABSTRACT

We present first results of a four-epoch VLBA survey for nonthermal emission toward all 556 compact radio sources previously identified in a deep VLA survey of the Orion Nebula Cluster (ONC). We identify VLBA counterparts toward an unprecedented 123 sources. Of these, 41 do not have X-ray counterparts, of which 34 also do not display near-infrared counterparts. Since these cannot be explained by extragalactic background sources, this suggests a component of the ONC population of young stellar objects that are too deeply embedded for even X-rays to be detectable. We find pervasive variability and detect even most of the highest-S/N sources in only one out of four epochs. Neither a negative spectral index nor extreme variability in the VLA data is a good predictor of a VLBA detection.

Keywords: astrometry — radiation mechanisms: non-thermal — stars:formation

1. INTRODUCTION

Even very early stages of star formation are associated with high-energy processes (e.g., Feigelson & Montmerle 1999). In addition to thermal X-ray emission, mostly from coronal hot plasma, young stellar objects (YSOs) have been observed to display both thermal free-free radio emission from ionized material in their vicinity and also non-thermal (gyro)synchrotron emission from electrons gyrating in magnetic fields (e.g., Güdel 2002). The latter is akin to scaled-up coronal-type activity, and it is often orders of magnitude more luminous than activity on our Sun. To reach these energies, the magnetic structures involved may be rooted in the YSO, but could also connect the star and its protoplanetary disk.

Observationally, it can be difficult to disentangle free-free and non-thermal emission, since they can arise from small scales, and they will often both occur in the same object. There are four main diagnostics that can be used to identify the emission mechanism. First of all, polarization will indicate gyrosynchrotron (circularly polarized) and synchrotron (linearly polarized) radiation. Then, the radio spectral index $S_\nu \propto \nu^\alpha$ can provide information as well, but it will often be ambiguous. Third, variability can be an indication, with rapid variability a sign of non-thermal emission (on timescales as short

as a few minutes, e.g. Forbrich et al. 2017), but there is again some ambiguity on intermediate timescales. Fourth, radio brightness temperature is a rarely employed but powerful indicator, since this technique allows us to select sources with brightness temperatures that are above that of thermal emission. This can naturally be accomplished by using Very Long Baseline Interferometry (VLBI), with which it is thus possible to filter out any thermal emission, enabling a census of nonthermal radio emission that remains largely unaffected by thermal radio emission. Apparent brightness is inversely proportional to the synthesized beam size for an unresolved source, and for milli-arcsecond resolution VLBI observations in C-band (4–8 GHz), even faint detections have corresponding brightness temperatures of several 10^6 K, well above possible values of free-free emission ($\approx 10^4$ to 10^5 K), even more so when considering that this is a lower limit. Even at this high resolution, the stellar radio emission remains unresolved, with a synthesized beam size corresponding to a linear scale of order 1 AU in our case. Overall, the two most useful indicators thus are polarization and brightness temperature.

In recent years, it has become possible to study populations of radio stars at unprecedented sensitivity, with a range of radio observatories. Our focus has been on observing YSOs in the Orion Nebula Cluster, the nearest young rich open cluster containing high-mass

stars ($d \sim 400$ pc; Menten et al. 2007; Kounkel et al. 2017). Altogether, the ONC has 3500 stellar members that formed less than 2 Myr ago (Hillenbrand et al. 2013), many of which emit X-rays (e.g., Getman et al. 2005a). Radio emission from YSOs in the ONC and the nearby Kleinmann-Low nebula was first observed when the NRAO Very Large Array became available (Garay et al. 1987; Churchwell et al. 1987), and prior to the VLA expansion, 77 radio sources had been observed in this cluster (Zapata et al. 2004). After the VLA expansion was completed, we obtained a deep pointing with what is now called the Karl G. Jansky Very Large Array, which allowed us to identify 556 radio sources in the ONC (Forbrich et al. 2016). Our analysis revealed extreme variability for many objects, strongly suggesting non-thermal emission (Forbrich et al. 2017). While this analysis included the derivation of in-band spectral indices for the brightest sources, it has been impossible so far to extract reliable wideband polarization information across the entire primary beam of this deep pointing.

To obtain a more reliable census of the incidence of non-thermal emission, and to then use this information for a proper motion census of the inner ONC, we have utilized the upgrade of the NRAO Very Long Baseline Array (VLBA). Crucially, this upgrade not only brought a significantly improved sensitivity, particularly in the C-band, but also the advent of the DiFX software correlator (Deller et al. 2007, 2011). Previously, correlation was limited to at most a few sources per experiment (e.g., Menten et al. 2007), but with the software correlator, it has become possible to correlate *all 556 sources* that we identified in our VLA data, in a near-identical primary beam. It is thus possible to obtain an unbiased dataset for which no assumptions need to be made on which sources are most likely to show non-thermal emission.

In this paper (Paper I) we address the incidence of non-thermal radio emission in 556 VLA-identified sources in the ONC, based on four separate observing epochs. An accompanying second paper (Paper II; Dzib et al. 2020, *subm.*), discusses the proper motion measurements of a subsample of our sources with detections in multiple epochs and how these complement *Gaia* results in a region that contains optically invisible deeply embedded objects and parts of which show bright nebulosity. A third paper will discuss variability and polarization information extracted from our dataset.

2. OBSERVATIONS AND DATA REDUCTION

We have observed the ONC with the VLBA on four occasions. The first observation was carried out on 2015

October 26 (BF117). In a follow-up program (BF123), three more observations were obtained on 2017 October 26 and 27 and on 2018 October 26. This experiment thus was designed to eliminate the effect of parallax by always observing at the same time of year. Note that we added a repeat epoch in 2017 to evaluate the effects of short-timescale variability (i.e., within a day). Identical observing setups were used, as described below, but antenna availability differed between epochs. For an overview about key parameters of the observations used here, see Table 1.

Observations were carried out in C-band at 2 Gbps in dual polarization with an aggregate bandwidth of 256 MHz in a frequency range of 7.068 to 7.324 GHz, using the Roach board-based Digital Backend with its Polyphase Filter Bank. 16 baseband channels in the upper sideband with 32 MHz bandwidth each were recorded with each band recorded in both LCP and RCP. To improve ionospheric calibration, the observations were interspersed with three sets of dual-frequency (4–8 GHz) geodetic observations (‘blocks’) of 30 min duration each (see Reid & Brunthaler 2004 for a related discussion), scheduled at the beginning and end of the observing run and in-between the science observations. The pointing position, $05^{\text{h}}35^{\text{m}}14^{\text{s}}.479 - 05^{\circ}22'30''.57$ (J2000), was the same as that used in our deep VLA observations (Forbrich et al. 2016). The phase calibrator for rapid switching was J0541–0541, at an angular distance of 1.6° , where 40 sec on the phase reference source were followed by 120 sec on the ONC position. The resulting on-source time was about 4.7 hours in each of the epochs. Due to differences in antenna availability, the (u, v) coverage varies slightly from epoch to epoch, with typical synthesized FWHM beam sizes listed in Table 1. The projected minimum baseline corresponds to about $3 \text{ M}\lambda$ (~ 125 km), while the maximum baseline length depends on the availability of the antennas at Mauna Kea and/or St Croix.

In terms of spectral coverage, our VLBA observations thus have been recording a subset of the bandwidth that was also recorded in our VLA experiment, albeit at a lower nominal sensitivity. While the concatenated VLA data have a nominal sensitivity of $3 \mu\text{Jy bm}^{-1}$, often not reached due to remnant emission of the largely filtered out but bright nebula, the nominal sensitivity of the VLBA images is $30 \mu\text{Jy bm}^{-1}$, but with a synthesized beam size that is ~ 100 smaller (see below) and no remnant extended structure. This nominal sensitivity varies somewhat from epoch to epoch, not least due to different numbers of available antennas. Given the wider band of the VLA C-band observations, even though it encompasses the frequency range covered here, the primary

beam of the corresponding VLA experiment is slightly larger than that of the VLBA experiment, depending on the frequency considered.

While our VLA study has already demonstrated the occurrence of extreme variability in this sample (Forbrich et al. 2017), we can obtain a few baseline comparisons to estimate how many sources may be detected in the VLBA data. First of all, 508 out of the 557 targets are located within the nominal VLBA primary beam (FWHM) at the observing frequency. Assuming that all of these are both nonthermal (i.e., detectable by VLBI) and non-variable (i.e., at the same flux level as during the VLA observations), which in combination is very unlikely, we would expect 98 sources to be detected above a signal-to-noise ratio, S/N, of 6.5, our sensitivity cut-off (see below). The actual number count will primarily depend on the fraction of VLA sources that have nonthermal emission and show variability. Already the extreme variability exhibited by some of the sources of our sample when observed with the VLA (Forbrich et al. 2017) underscores the limited meaningfulness of using a time-averaged flux density as an S/N threshold.

We have used the multi-object capabilities of the DiFX software correlator (Deller et al. 2007, 2011) to obtain VLBA data for all 556 compact VLA sources. Starting with the follow-up experiment BF123, we additionally correlated at the position of COUP 672 as the 557th target, following its detection at radio frequencies by Dzib et al. (2017).

Data reduction was carried out using standard procedures using the NRAO Astronomical Image Processing System¹ (AIPS). In a first step, systematic delays were removed based on measurements of the ionospheric total electron content, as provided for the time of the observation by Global Positioning System data, and all data were corrected using the latest USNO Earth orientation parameters. Subsequently, residual delays from clock drifts and zenith atmospheric delays were measured using the geodetic blocks and removed. This step involved the AIPS routine DELZN to estimate clock delays. Electronic delays and differences among the IF bands were then removed using observations of the strong calibration source J0530+133. Finally, we interpolated the phases of the reference source and applied this identical calibration to all separately correlated science targets. These steps were repeated for all four epochs considered here.

3. DATA ANALYSIS

3.1. Source detection

To check for source detections, all 557 targets in all four epochs were imaged using AIPS in Stokes I , resulting in more than 2200 images. To search for peaks in a wide field, this first set of images consisted of images of size 2048^2 pixels with a pixel size of 0.5 mas, i.e., we mapped areas of about a square arcsecond, centered at the VLA positions, using natural weighting. The smallest synthesized beam of $\sim 1.2 \times 2.8$ mas was slightly undersampled with at least two pixels per half-power beam width in each axis, and the main goal was to search for detections in a wide area. This resolution corresponds to AU scales at the distance of the ONC, and any coronal-type emission should thus be unresolved.

For a second round of imaging, we then conservatively selected peaks above a threshold of $S/N = 5.5$, as determined from the peak pixel value and the pixel rms in the images produced with AIPS, to be imaged in greater detail. We here utilize the work of Herrera Ruiz et al. (2017), who analyzed the role of noise in the source detection process when analyzing VLBI images of faint radio sources in the COSMOS field. While that study was obtained at a frequency of 1.4 GHz, the COSMOS field lends itself more easily to a systematic study of detection probabilities than the comparatively crowded ONC. These authors found clear signs of non-Gaussian noise when going to lower S/N detection levels (see also Middelberg et al. 2013). The joint probability of finding a false positive or a chance detection within $0''.4$ of a VLA source was estimated to be 19%, 0.2%, and 0.02% for cut-offs of $S/N=5$, 5.5, and 6, respectively, clearly a non-Gaussian progression. They concluded that a cut-off at $S/N = 7$ means that the false-positive detection rate can be ignored.

In our case, we have a less stringent constraint on the offsets between the VLA and VLBA positions than if we expected constant positions, since significant proper motions may have occurred in our sources during the course of this experiment, and even different components of multiple systems may be detected in some epoch(s), but not in others. Our search area is approximately 2.5 times larger than that of Herrera Ruiz et al. (2017). We pick a cut-off of $S/N=6.5$ for an estimated false-positive rate of ~ 0.1 sources across the full sample and four epochs. The nominal Gaussian expectation at this significance level would be 0.02 false detections, leaving a factor of a few for any non-Gaussian noise, while still ensuring a low false-positive rate.

To illustrate the need for a cut-off at this relatively high S/N level, we note that all images of the first epoch (to give an example) contain peaks with $S/N > 4.6$, and 457 maps have peaks with $S/N > 5$, clearly pointing at

¹ <http://www.aips.nrao.edu/>

Table 1. Observing log

Epoch	Date, Time (UT)	Beam ¹	Antennas
BF117	2015 Oct 26, 06:25–14:23	4.7× 1.6	8 (no MK, HN)
BF123A	2017 Oct 26, 06:23–14:21	4.4× 1.3	9 (no SC, PT ² , HN ²)
BF123B	2017 Oct 27, 06:19–14:17	4.1× 1.4	8 (no SC, HN, PT ²)
BF123C	2018 Oct 26, 06:24–14:22	2.8× 1.2	10

¹Synthesized beam (FWHM), in milliarcseconds

²operational, but flagged during processing

the presence of noise peaks. We also note that the maximum number of independent elements in our images is the number of enclosed FWHM synthesized beams. Our large images of four million pixels typically contain between 120,000 and 270,000 synthesized beam areas. As a result, within our complete sample of 557 targets, we would expect about one spurious detection due to the chance appearance of a noise peak at $S/N > 5.5$ by Gaussian noise alone, motivating the choice of a higher cut-off.

For the brightest peaks thus identified we then produced fully sampled images using CASA. A target position identified in one epoch was imaged in all four epochs. Here, we again used image sizes of 2048^2 pixels, but with a pixel size of 0.05 mas, i.e., we mapped areas of 0.1×0.1 arcseconds, using natural weighting. A total of 171 source positions showed peaks with $S/N > 5.5$ and were thus imaged in this way, with a typical image rms sensitivity of $21 \mu\text{Jy bm}^{-1}$.

We additionally concatenated the data of the two epochs separated by just one day, BF123A and BF123B, that were only separated by one day to additionally search for detections at higher sensitivity, and a few additional sources beyond those identified in the analysis below were identified. While our discussion is otherwise limited to the individual epochs, we highlight these additional sources in our discussion below.

Several factors complicate the source detection: 1) many sources are likely variable, particularly given the nonthermal nature of the emission, 2) unknown but significant proper motions between epochs (except for BF123AB) make it impossible to look for coincident detections, 3) the target positions are only known at about 100 times lower resolution with different spatial filtering properties; the VLA detections could split into multiple VLBA sources, and 4) given the overall number of pixels, there is an increased chance of detecting noise peaks as seemingly significant sources.

Visual inspection of the results quickly highlighted the fact that the detected sources are highly variable, as can

be expected from nonthermal emission, which is underlining the value of multiple observing epochs for this experiment. We adapted our detection criteria accordingly by only requiring one detection above the cut-off of $S/N > 6.5$.

4. RESULTS AND DISCUSSION

Among 557 targets we report 123 detections, including 12 identified in the concatenated epoch BF123AB. Next to the 386 sources with peaks of $S/N < 5.5$ and thus not selected for detailed imaging, the remaining 48 sources out of the imaged sample of 171 sources are considered to be nondetections. Out of 557 targets, we thus have 123 detections and 434 nondetections. The detections are listed in Table 2, where we also list additional information including on the identification of X-ray and NIR counterparts and on the nominal angular separation of these detections from the VLA positions. The number of detections is greater than expected from scaling the VLA flux densities alone (98), which is probably due to the fact that these flux densities, averaged over almost 30 h, underestimate the flux density observable during flares.

It is also interesting to consider the positional offset when compared with the nominal VLA positions, based on observations obtained in 2012 (Forbrich et al. 2016). While a number of positions fall within a few 10 mas of the nominal VLA position (from 2012), more extreme examples include the detection at $S/N = 7.9$ in source 300, at a distance of 580 mas from the expected position, corresponding to about 230 AU at the distance of the ONC, and plausibly a component of a multiple system. This highlights why no cut-off in angular separation has been applied within the imaged areas.

A full discussion of the positions and proper motions of the detected sources is presented in Paper II. Here, we are primarily interested in quantifying the number of VLBA detections in our large VLA sample. The most striking result, enabled by studying four separate epochs, is the enormous influence of variability, a clear

sign of nonthermal emission, on the detection count. Additionally, we detect, on two occasions, *two* radio sources toward a single VLA source on VLBA scales (sources 177 and 414), adding to the sample of radio binaries in the ONC, and underscoring the potential for significant positional offsets when compared to the nominal VLA position. These are discussed in Paper II.

We illustrate the impact of variability on this detection experiment by highlighting the number of detections per source among the four epochs, as a function of S/N cut-off. In Figure 1, we plot the number of nominal detections, defined as peaks in the search area per source, as a function of several different S/N cutoffs, color-coding the *number* of detections among the four epochs. Not too surprisingly, the overall number of detections decreases for higher S/N cutoffs. However, even in the highest-S/N group with $S/N > 7.5$, most sources reach this level of significance in just one out of four epochs: Out of a total of 55 sources with a maximum S/N per epoch of $S/N > 7.5$, 37 reach this level in just one epoch, and only 8 sources reach it in all four epochs.

A particularly instructive look at the role of variability comes from a comparison of epochs BF123A and BF123B, which were observed on two subsequent days. Out of 28 sources that were detected at $S/N > 6.5$ in BF123A, only eleven sources were detected at $S/N > 6.5$ on the next day.

4.1. Source identification

As discussed in Forbrich et al. (2016), the multi-wavelength identification of the VLA sources is not entirely straightforward. While most of them are expected to be YSOs emitting nonthermal radio emission, the sample also contains sources with thermal radio emission, for example arising from protoplanetary disks externally photoionized by UV radiation from the ONC's most luminous O-type star θ^1 Ori C, the so-called *proplyds* (O'dell et al. 1993), or from outflows and jets (e.g., Anglada et al. 2018).

A correlation with X-ray data is the best way of identifying emission from YSOs, given the reduced extinction cross section of the interstellar medium in the X-ray range and the lack of source confusion due to nebulosity in the Orion Nebula, which in comparison lowers the sensitivity of infrared observations. Already when discussing the VLA sample, we had correlated the radio sample with the deep X-ray catalog from the Chandra Orion Ultra-deep Project (COUP, Getman et al. 2005b) to identify YSOs with a search radius of $0''.5$, while keeping in mind that due to variability and extinction, an X-ray non-detection could still be related to a YSO. We use the VISION survey to identify near-infrared coun-

terparts (Meingast et al. 2016). X-ray and infrared non-detections do not necessarily rule out ONC members, if the extinction is very high (affecting both X-rays and infrared emission) or if bright emission from the nebula significantly reduces the sensitivity in the infrared. One example is the flare source from Forbrich et al. (2008), from which no infrared emission was detected, and only a brief X-ray flare enabled the identification as a YSO.

One hypothesis would thus be that the VLBI experiment preferentially singles out VLA sources with X-ray counterparts, since this would increase the likelihood of detecting coronal activity. We have included the associated COUP sources from Forbrich et al. (2016) in Table 2, keeping in mind that particularly in the case of multiple systems, the X-ray and radio emission may be unrelated. Near-infrared information is included as well.

Interestingly, from among the 123 detections, a considerable subset of 41 sources (or one third) do *not* exhibit an X-ray counterpart in the COUP survey. Overall, however, the X-ray incidence rate is two thirds, correspondingly, which is higher than that of the full VLA sample at 46%. It is worth noting that the highest S/N of an X-ray non-detection occurs in source 11, at $S/N = 8.7$, and all remaining X-ray non-detections have VLBI detections with a peak S/N ranging from 6.5 to 8.7. This range in detection significance overlaps with that of VLBI sources with X-ray detections, and the non-detections thus are unlikely to be entirely due to the relative sensitivity of *Chandra* and the VLBA to detecting YSOs. Near-infrared data do not significantly change this picture, as 34 out of the 41 sources without X-ray counterparts also do not display NIR counterparts while 72 of the 82 sources with X-ray counterparts show near-infrared detections.

Some of the VLBI detections without multi-wavelength counterparts could be extragalactic background sources. However, in the entire VLA C-band beam, we would only expect at most three extragalactic sources at $S > 0.195$ mJy (or 6.5 times the typical rms of the observations reported here), based on Windhorst et al. (1993). An additional perspective on these questions will be afforded by the analysis of proper motions, but the intriguing conclusion is that most of these targets belong to the YSO population of the ONC even though they so far have remained undetected in X-rays.

While X-ray data provide a means of identifying YSO counterparts to the radio sources, extensive literature exists also on spectral types and YSO evolutionary classes in the ONC, even if the X-ray data arguably provide the most complete census. The main problem is

that in various wavelength regimes, the Orion Nebula’s bright extended emission precludes the collection of data for various sources, which often means that only limited non-radio band information is available on a given object. In particular, note that only a fraction of the ONC’s member stars could be measured by *Gaia* (see Paper II). For many Orion sources, there are indications of multiplicity, which impacts this study in two different ways: 1) the attribution of a spectral type to a the radio emitting stellar component may be ambiguous, and 2) positional offsets would be expected if just one component in a multiple system is detected by VLBI.

As discussed in Forbrich et al. (2016), the VLA radio sample comprises sources with spectral types ranging from M to O as catalogued most recently by Hillenbrand et al. (2013), and the same is true for the VLBI sample (when assuming that actual counterparts are compared). Spectral types of 56 of our targets have been reported by Hillenbrand et al. (2013). Additionally, eight of our VLBI detections are listed, within our search radius of $0.5''$, in the X-ray/NIR study of the inner ONC by Prisinzano et al. (2008), who determined evolutionary classes for the X-ray detected YSOs in the ONC, all T Tauri stars. Six out of these are listed as class III sources, and two as class II sources. However, with fewer than 5% of even our input VLA sample having counterparts in Prisinzano et al. 2008, an assessment of detection rates in different YSO evolutionary stages cannot be obtained at this time. Spectral types and protostellar classes, where available, are listed in Table 2.

It is also worth considering constraints from the deep VLA observations that we could have used to select candidate nonthermal targets if it would have been impossible to conduct an unbiased VLBA survey. Interestingly, the VLBA detections reported here do not correlate strongly with observable VLA characteristics, underlining the value of this unbiased survey. Other than previous VLBA detections (Menten et al. 2007; Kounkel et al. 2017), we could have selected the subset of VLA sources with significantly negative in-band spectral indices in Forbrich et al. (2016). As discussed in our VLA paper, out of 170 sources with reliable spectral indices, the best candidates for nonthermal emission are the 17 sources therein that have negative spectral indices with a significance of at least 3σ . Remarkably, only two of these 17 sources ([FRM2016] 127 and 148) show up in our list of VLBA detections, while overall 53 out of the 170 sources with reliable spectral indices have been detected with the VLBA. Similarly, we could have picked the 13 extremely variable VLA sources (varying by more than an order of magnitude on short timescales) from Forbrich et al. (2017), and here the VLBA detec-

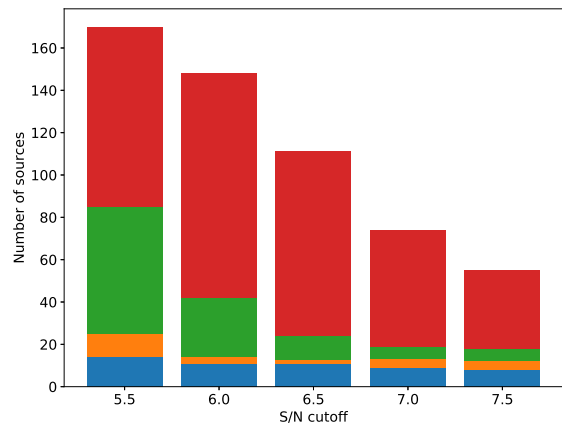


Figure 1. Number of sources detected above a given S/N threshold, color-coded by number of detections among four epochs (red=1, green=2, orange=3, blue=4).

tion rate is somewhat higher: seven out of these 13 sources ([FRM2016] 53, 98, 189, 254, 319, 414, and 515) are VLBA detections in our experiment, in addition to the flare source from Forbrich et al. (2008), which is also detected ([FRM2016] 198). While the detection of non-thermal emission with the VLBA is unambiguous, the intermittent nature of nonthermal emission means that multiple epochs of observations may be required in order to characterize the population of stars that show non-thermal emission, and any observable that is impacted by this variability is not a good predictor for nonthermal emission at a different time. Extreme variability at least appears to be a better indicator of nonthermal emission than negative spectral indices in this case, where the VLA spectral indices are an average out of almost 30 hours of observations, perhaps not sufficiently accounting for the intermittent nonthermal variability.

5. SUMMARY AND CONCLUSIONS

We present first results of multi-epoch VLBA follow-up of 556 VLA radio sources in the ONC, involving four epochs obtained over a time interval of three years, while eliminating the role of parallax motions. The first goal is to quantify the nonthermal population as defined by the set of VLBI detections of sources in our VLA catalog. Across four epochs, we find an unprecedented total of 123 detections. We find strong variability, as may be expected from nonthermal coronal-type emission, and very few bright sources are detected in all epochs. The incidence of X-ray counterparts among the VLBI sample, at two thirds, is significantly higher than in the VLA sample, indicating that the VLBI observations preferentially single out young stellar sources. However, 41 of

the sources do not have X-ray detections, and 34 of those also do not have near-infrared detections, hinting at a population of radio-detected YSOs that remained undetected in X-ray observations due to variability, extinction, or both. When compared with indications of non-thermal emission derived from our previous deep VLA data, we find that neither in-band spectral indices nor extreme variability would have been a good predictor of our VLBA detections, even if significant variability works better in this regard than the negative spectral indices. This again underlines the value of now being able to conduct unbiased surveys with the VLBA due to the advent of software correlation.

ACKNOWLEDGMENTS

We thank the anonymous referee for helpful and constructive comments that lead to an improved presentation of our results. The National Radio Astronomy Observatory is a facility of the National Science Foundation operated under cooperative agreement by Associated Universities, Inc.

Table 2. List of VLBA detections in the Orion Nebula Cluster

[FRM2016]	COUP	VISION NIR ¹	$N_{S/N>6.5}$	$(S/N)_{\max}$	Ep. ²	Sep. (mas) ³	Notes ⁴
2	107	05345597-0523130	2	61.8	C	185	class III; K1-K4
10	262	05350628-0522027	1	13.9	C	26	class III; K5
11	–	–	1	8.7	B	216	
14	283	05350727-0522266	1	6.8	A	523	M4.5
18	338	05350968-0523559	2	15.4	7	43	
21*	343	05350977-0523269	1	8.6	AB	12	class III; K4-M0
22	342	05350977-0521284	1	18.0	B	12	M0, K5-K7
24	350	05350990-0523385	1	6.7	7	291	
25*	–	–	0	6.8	AB	299	
30	363	05351026-0521571	1	6.7	A	215	M5.5
32*	378	05351050-0522455	0	6.7	AB	16	K6-M2
35*	390	05351062-0522560	0	7.1	AB	444	
37	394	05351073-0523446	1	7.0	B	79	K2-M0
42	–	05351093-0523267	1	7.8	C	260	
47*	–	–	0	6.7	AB	551	
53	427	05351156-0524481	1	12.9	C	59	
55	–	–	1	7.2	B	335	
64	444	05351172-0525128	1	7.3	B	49	
66	450	05351180-0521493	4	78.7	A	8	
70	–	–	1	7.2	B	464	
72	–	–	1	7.6	B	378	
75	465	05351212-0524338	1	7.0	C	380	M1-M2e
86*	–	–	0	8.1	AB	173	
93	504	05351285-0521340	1	17.0	7	5	class II
98	510	–	1	6.9	7	372	
122	–	–	1	6.5	B	526	
127	551	05351352-0522196	1	7.1	B	387	K-M1
129	–	–	1	7.9	B	448	
130	554	05351358-0523552	4	144.7	C	26	
133	–	–	1	8.2	B	199	
135	–	–	1	6.9	A	405	
137	–	–	2	7.1	B	279	

Table 2 *continued*

Table 2 (continued)

[FRM2016]	COUP	VISION NIR ¹	$N_{S/N>6.5}$	$(S/N)_{\max}$	Ep. ²	Sep. (mas) ³	Notes ⁴
148	593	05351392-0523202	1	7.4	A	572	
149*	–	–	0	8.9	AB	425	
154	594	–	3	78.9	C	20	
158	602	05351405-0523384	2	8.2	A	19	M3
161	598	–	1	6.6	7	240	
167	608	–	1	6.5	C	359	
170	–	–	1	7.1	C	520	
176	–	–	1	6.6	C	546	
177	625	–	2	26.0	C	13	
182	–	–	1	7.7	B	557	
184	639	–	4	49.9	C	16	
188	–	–	1	6.6	A	476	
189	640	–	1	8.3	7	16	
196	648	(det)	1	15.9	7	23	K3-M2
197	645	05351465-0520424	1	6.7	A	166	class II
198	647	–	2	9.0	C	8	Orion Radio Burst Source (ORBS)
203*	–	05351472-0522296	0	8.3	AB	9	
205	–	–	1	6.7	7	522	
211	662	–	4	24.5	A	16	
212	670	05351492-0522392	1	35.1	7	14	K3-M2
222	689	05351526-0522568	1	7.4	B	453	G6-K7
227	–	–	1	6.8	B	176	
230	–	–	1	6.8	C	472	
232	–	–	1	7.5	C	309	
240	717	05351552-0523374	1	7.0	7	122	K
241	718	(det)	3	59.1	C	54	K4-M1
242*	–	–	0	6.8	AB	233	
249	734	05351576-0523384	1	6.6	C	514	
250	732	(det)	4	80.6	C	10	B5-B8+G0-G5
254	745	05351582-0523143	4	214.6	C	37	O9-B1.5
273	–	05351608-0523278	1	7.3	C	299	
285*	783	05351619-0521323	0	7.7	AB	508	M4.5
300	801	05351638-0524032	1	7.9	7	580	K4-K7
303	806	05351642-0522121	1	7.0	B	271	
314	–	–	2	7.7	7	496	
319	828	05351676-0524042	4	11.9	7	23	K2-K6
321	827	05351677-0523280	1	7.6	A	539	
326	841	05351693-0522098	1	10.8	B	429	
327	–	–	1	7.3	7	447	
335	856	05351706-0523397	1	6.8	A	345	K5e
339	–	05351712-0524344	1	6.8	C	139	
343	867	05351721-0521317	1	8.2	7	21	K3-K7
347	876	05351735-0522357	1	6.9	C	360	K0-K2,K2-K4
350	874	05351739-0522036	2	14.6	C	16	
357*	896	05351750-0521062	0	7.7	AB	162	
360	897	05351755-0521455	1	6.7	B	420	
364	–	05351768-0523410	1	7.0	B	277	K-M

Table 2 continued

Table 2 (continued)

[FRM2016]	COUP	VISION NIR ¹	$N_{S/N>6.5}$	$(S/N)_{\max}$	Ep. ²	Sep. (mas) ³	Notes ⁴
367	–	05351773-0524437	1	6.9	A	611	
373*	–	–	0	6.8	AB	277	
378	932	05351794-0522455	4	153.9	C	13	G-K3
382	942	05351803-0522054	1	15.6	C	37	G-M2
389	956	05351820-0523359	1	7.6	7	115	G4-K3
398	–	–	1	6.5	C	514	
400	965	05351836-0522374	4	204.6	C	17	G8-M2
402	963	05351839-0520204	1	6.6	C	36	class III; K8-M1.5, M1.5-M3, M3-M4
408	–	–	1	6.7	B	663	
414	985	05351866-0520337	4	15.5	C	27	F8-K4
426	–	–	1	6.7	B	645	
435	1023	05351921-0522507	1	12.4	B	12	
440	–	–	1	7.1	C	281	
456	–	–	1	7.4	B	503	
457	1071	05352005-0521059	1	6.7	A	332	K
459	1083	05352013-0521336	1	21.3	7	20	class III; <M0
462	1087	05352016-0526390	1	16.7	C	130	mid-G-early-K
466	1090	05352021-0520569	2	39.3	B	57	F7-K3
467	1091	05352027-0525040	1	7.2	B	560	
468	1100	05352039-0522136	1	11.7	C	21	class III; M0, M1
470	–	–	1	6.5	C	86	
477	1110	05352064-0522455	1	6.8	C	372	M4.5
480	1116	05352072-0521443	2	22.1	C	6	B
485	1130	05352104-0523490	4	36.2	B	38	G8-K5
501	1184	05352209-0524328	1	6.7	A	579	
508	1205	05352232-0524142	1	6.9	C	413	K5-M1.5
509	–	–	1	6.7	C	367	
512	–	–	1	7.7	B	527	
514	–	05352283-0525476	1	7.7	B	234	M5.5
515	1232	05352289-0524578	1	6.6	C	80	
520	1249	05352349-0520017	1	9.3	C	64	
521	1262	05352359-0525264	1	7.3	7	372	M3-M3.5e
522	1260	05352365-0523463	1	8.9	B	314	M1
525	1275	05352398-0525098	1	7.8	A	561	M1
526	1276	05352403-0523138	1	7.2	7	155	
527	1281	05352426-0525187	1	7.6	B	315	K0-K6
530	1289	05352447-0524010	1	6.9	C	148	M1-M3:
534	–	–	1	7.8	B	440	
535	1313	05352503-0524384	1	6.7	C	315	
537	1311	05352508-0523467	1	9.8	A	79	K2-K5
547	1360	05352639-0525007	1	14.8	B	98	B0-B2
552	1428	–	1	7.5	B	208	
555	1473	05353143-0525162	1	6.6	A	422	B3-B6
(557)	672	05351494-0523393	2	10.6	B	–	K5-M2

Table 2 continued

Table 2 (*continued*)

[FRM2016]	COUP	VISION NIR ¹	$N_{S/N>6.5}$	$(S/N)_{\max}$	Ep. ²	Sep. (mas) ³	Notes ⁴
-----------	------	-------------------------	---------------	----------------	------------------	-------------------------	--------------------

¹From Meingast et al. (2016), unlisted detections (e.g., due to crowding) listed as '(det)'.

²Epoch of $(S/N)_{\max}$: BF117 (7), BF123ABC (A,B,C), or the concatenated epoch BF123AB (AB).

³Separation between detection and nominal VLA position, in milliarcseconds

⁴Previous identifications: YSO classes from Prisinzano et al. (2008) and spectral types summarized from Hillenbrand et al. (2013). Note that these are for counterparts within $0.5''$ and do not necessarily represent counterparts of the radio sources, particularly in the case of multiple systems. See Paper II for detailed discussion.

NOTE—Source positions are presented in Paper II. Sources with an asterisk only fulfill the selection criterion in the concatenated epoch BF123AB. The listing of peaks above S/N threshold does not include this concatenated epoch. All sources have four observations each, except for source 557 (see text), which was not correlated in the first epoch (BF117) and which is not listed in Forbrich et al. (2016). Source 198 is the “Orion Burst Source” in the Kleinmann Low nebula, for which a strong outburst at 22.2 GHz was reported by (Forbrich et al. 2008).

REFERENCES

- Anglada, G., Rodríguez, L. F., & Carrasco-González, C. 2018, *A&A Rv*, 26, 3, doi: [10.1007/s00159-018-0107-z](https://doi.org/10.1007/s00159-018-0107-z)
- Churchwell, E., Felli, M., Wood, D. O. S., & Massi, M. 1987, *ApJ*, 321, 516, doi: [10.1086/165648](https://doi.org/10.1086/165648)
- Deller, A. T., Tingay, S. J., Bailes, M., & West, C. 2007, *PASP*, 119, 318, doi: [10.1086/513572](https://doi.org/10.1086/513572)
- Deller, A. T., Brisken, W. F., Phillips, C. J., et al. 2011, *PASP*, 123, 275, doi: [10.1086/658907](https://doi.org/10.1086/658907)
- Dzib, S. A., Rodríguez, L. F., Loinard, L., et al. 2017, *ApJ*, 834, 139, doi: [10.3847/1538-4357/834/2/139](https://doi.org/10.3847/1538-4357/834/2/139)
- Feigelson, E. D., & Montmerle, T. 1999, *ARA&A*, 37, 363, doi: [10.1146/annurev.astro.37.1.363](https://doi.org/10.1146/annurev.astro.37.1.363)
- Forbrich, J., Menten, K. M., & Reid, M. J. 2008, *A&A*, 477, 267, doi: [10.1051/0004-6361:20078070](https://doi.org/10.1051/0004-6361:20078070)
- Forbrich, J., Reid, M. J., Menten, K. M., et al. 2017, *ApJ*, 844, 109, doi: [10.3847/1538-4357/aa7aa4](https://doi.org/10.3847/1538-4357/aa7aa4)
- Forbrich, J., Rivilla, V. M., Menten, K. M., et al. 2016, *ApJ*, 822, 93, doi: [10.3847/0004-637X/822/2/93](https://doi.org/10.3847/0004-637X/822/2/93)
- Garay, G., Moran, J. M., & Reid, M. J. 1987, *ApJ*, 314, 535, doi: [10.1086/165084](https://doi.org/10.1086/165084)
- Getman, K. V., Feigelson, E. D., Grosso, N., et al. 2005a, *ApJS*, 160, 353, doi: [10.1086/432097](https://doi.org/10.1086/432097)
- Getman, K. V., Flaccomio, E., Broos, P. S., et al. 2005b, *ApJS*, 160, 319, doi: [10.1086/432092](https://doi.org/10.1086/432092)
- Güdel, M. 2002, *ARA&A*, 40, 217, doi: [10.1146/annurev.astro.40.060401.093806](https://doi.org/10.1146/annurev.astro.40.060401.093806)
- Herrera Ruiz, N., Middelberg, E., Deller, A., et al. 2017, *A&A*, 607, A132, doi: [10.1051/0004-6361/201731163](https://doi.org/10.1051/0004-6361/201731163)
- Hillenbrand, L. A., Hoffer, A. S., & Herczeg, G. J. 2013, *AJ*, 146, 85, doi: [10.1088/0004-6256/146/4/85](https://doi.org/10.1088/0004-6256/146/4/85)
- Kounkel, M., Hartmann, L., Loinard, L., et al. 2017, *ApJ*, 834, 142, doi: [10.3847/1538-4357/834/2/142](https://doi.org/10.3847/1538-4357/834/2/142)
- Meingast, S., Alves, J., Mardones, D., et al. 2016, *A&A*, 587, A153, doi: [10.1051/0004-6361/201527160](https://doi.org/10.1051/0004-6361/201527160)
- Menten, K. M., Reid, M. J., Forbrich, J., & Brunthaler, A. 2007, *A&A*, 474, 515, doi: [10.1051/0004-6361:20078247](https://doi.org/10.1051/0004-6361:20078247)
- Middelberg, E., Deller, A. T., Norris, R. P., et al. 2013, *A&A*, 551, A97, doi: [10.1051/0004-6361/201220374](https://doi.org/10.1051/0004-6361/201220374)
- O’dell, C. R., Wen, Z., & Hu, X. 1993, *ApJ*, 410, 696, doi: [10.1086/172786](https://doi.org/10.1086/172786)
- Prisinzano, L., Micela, G., Flaccomio, E., et al. 2008, *ApJ*, 677, 401, doi: [10.1086/528842](https://doi.org/10.1086/528842)
- Reid, M. J., & Brunthaler, A. 2004, *ApJ*, 616, 872, doi: [10.1086/424960](https://doi.org/10.1086/424960)
- Windhorst, R. A., Fomalont, E. B., Partridge, R. B., & Lowenthal, J. D. 1993, *ApJ*, 405, 498, doi: [10.1086/172382](https://doi.org/10.1086/172382)
- Zapata, L. A., Rodríguez, L. F., Kurtz, S. E., & O’Dell, C. R. 2004, *AJ*, 127, 2252, doi: [10.1086/382715](https://doi.org/10.1086/382715)